

# RSC Advances



This is an *Accepted Manuscript*, which has been through the Royal Society of Chemistry peer review process and has been accepted for publication.

*Accepted Manuscripts* are published online shortly after acceptance, before technical editing, formatting and proof reading. Using this free service, authors can make their results available to the community, in citable form, before we publish the edited article. This *Accepted Manuscript* will be replaced by the edited, formatted and paginated article as soon as this is available.

You can find more information about *Accepted Manuscripts* in the [Information for Authors](#).

Please note that technical editing may introduce minor changes to the text and/or graphics, which may alter content. The journal's standard [Terms & Conditions](#) and the [Ethical guidelines](#) still apply. In no event shall the Royal Society of Chemistry be held responsible for any errors or omissions in this *Accepted Manuscript* or any consequences arising from the use of any information it contains.

## COMMUNICATION

# Hexamethylenetetramine mediated simultaneous nitrogen doping and reduction of graphene oxide for a metal-free SERS substrate

Cite this: DOI: 10.1039/x0xx00000x

Received 00th January 2012,  
Accepted 00th January 2012

Barun Kumar Barman and Karun Kar Nanda\*

DOI: 10.1039/x0xx00000x

www.rsc.org/

**We report a one-pot hydrothermal synthesis of nitrogen doped reduced graphene oxide (N-rGO) and Ag nanoparticles decorated N-rGO hybrid nanostructures from graphene oxide (GO), metal ions and hexamethylenetetramine (HMT). HMT not only reduces GO and metal ions simultaneously but also acts as the source for the nitrogen (N) dopant. We show that the N-rGO can be used as metal-free surface enhanced Raman spectroscopy (SERS) substrate, while the Ag nanoparticles decorated N-rGO can be used as effective SERS substrate along with a template for decorating various other nanostructures on N-rGO.**

Pristine, doped and nanoparticles (NPs) decorated graphene have gained great attention due to their extraordinary electronic, mechanical and thermal properties and their applications in various field such as electronics, optical sensors, energy storage application etc.<sup>1</sup> The performance is shown to be improved significantly when the graphene is modified by doping<sup>2,3</sup> or decorating with metal NPs.<sup>4</sup> For example, nitrogen doped graphene<sup>5</sup> and graphene decorated with metal/metal oxide NPs<sup>6</sup> can be an excellent catalyst for oxygen reduction reaction<sup>7</sup> and metal decorated graphene can be used for surface enhanced Raman spectroscopy (SERS),<sup>8-11</sup> reduction of nitrophenol,<sup>12, 13</sup> etc. The synthesis of doped and metal NPs decorated graphene with good control of size and structures is of paramount importance for specific applications. However, it is a challenge to synthesize nitrogen doped graphene or graphene decorated with metal NPs in large scale. Though several approaches such as micromechanical exfoliation of graphite,<sup>14</sup> chemical vapour deposition (CVD),<sup>15</sup> and epitaxial growth,<sup>16</sup> chemical reduction of graphene oxide (GO) to obtain reduced graphene oxide (rGO),<sup>17-19</sup> has the advantage of large scale production and cost effective. Similarly, simultaneous reduction and decoration of metal NPs is the most viable approach for the large scale synthesis of the hybrids. Simultaneous reduction of GO and nitrogen doping has also been achieved by heating GO in presence of ammonia,<sup>20</sup> chemical vapour deposition,<sup>21,22</sup> and hydrothermal and method.<sup>20-24</sup>

Here, we report the one-step synthesis of nitrogen doped rGO (N-rGO) and Ag NPs/N-rGO hybrids from GO by using hexamethylenetetramine (HMT). HMT acts as a reducing agent for both GO and Ag<sup>+</sup> ions and N source for doping. The overall chemical reactions are presented in Fig 1. We show that the N-rGO can be used as metal-free SERS substrates and SERS can further be enhanced by the presence of Ag NPs. We also show that the Ag NPs/N-rGO hybrid nanostructures can be used as effective template for decorating porous metallic nanostructures on N-rGO.

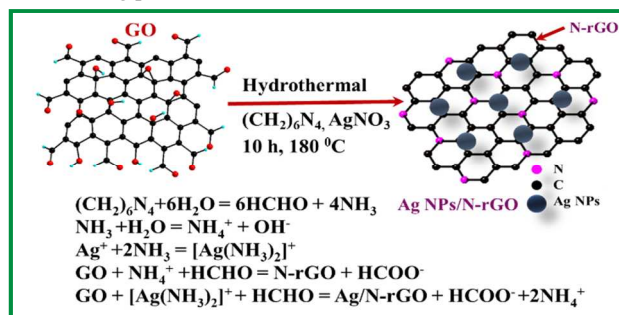


**Fig. 1** Schematic diagram and chemical equation of for Ag/N-rGO hybrids nanostructures by simultaneous reduction of both Ag<sup>+</sup> ions and GO followed by N doping in rGO.

In order to synthesize N-rGO, GO flakes along with HMT solution was taken in an autoclave and treated at 180 °C for 10 h in absence of any surfactant and reducing agent. We chose HMT ((CH<sub>2</sub>)<sub>6</sub>N<sub>4</sub>) for this reaction, which is a water-soluble, nontoxic, non-ionic and tetradentate cyclic ternary amine.<sup>22</sup> In aqueous medium, it releases hydroxyl ion, ammonia (NH<sub>3</sub>) and formaldehyde (HCHO). As a result GO gets reduced and doped by N simultaneously in presence of HCHO and NH<sub>3</sub>, respectively and finely we are getting black precipitation of N-rGO. Similarly, Ag NPs/N-rGO were obtained by taking GO, HMT and AgNO<sub>3</sub>. When Ag<sup>+</sup> ions are added, it formed 2-coordinate Ag(I) complex with the NH<sub>3</sub>. This complex can be further reduced by HCHO in the reaction

medium to form Ag NPs on the graphene sheet. The entire results suggest that HMT plays multiple roles in the reaction medium and the overall reactions for the one-step the synthesis of Ag NPs/N-rGO are provided in schematic **Fig. 1**. We also decorated Pd nanostructures on N-rGO substrate by sacrificing AgNPs by galvanic replacement reaction (GRR).

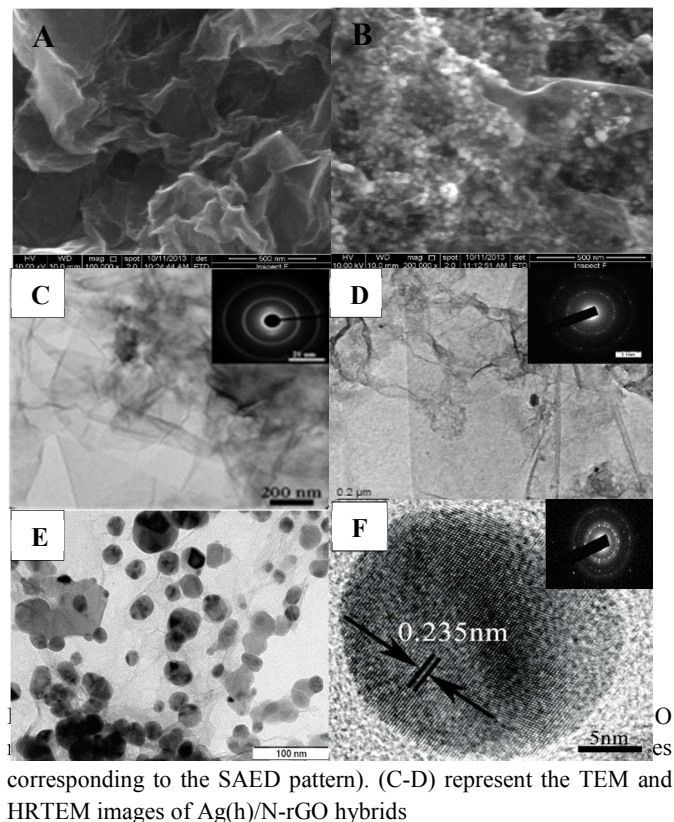


**Fig. 2** (A & B) show of SEM images of crumbled solid N-rGO and dense Ag NPs decorated N-rGO sheet. We have performed few more experiments in order to control the size and the density of the Ag NPs. When the  $\text{Ag}^+$  ions concentration in the reaction mixture is reduced, the density of Ag NPs gradually decreases and the size of the NPs increases as randomly aggregated, crumpled solid sheets as shown in **ESI-1**. **Fig. 2** (C & D) display the TEM images of GO and N-rGO sheet and the inset images display the corresponding SAED patterns. Transformation from the ring-like pattern of GO to clear individual spot in the SEAD pattern of N-rGO suggests the reduction GO. The loss of oxygen containing functional group helps to regain the crystalline graphitic nature in N-rGO from the polycrystalline nature of GO.<sup>25</sup> The size of Ag NPs as obtained from TEM image (**Fig. 2** E) is in 16-26 nm range and the average diameter is  $\sim 22$  nm. The d-spacing is 0.235 nm of AgNPs is calculated from **Fig. 2** (F) and single crystalline as confirmed from the SAED pattern<sup>26, 27</sup> Hereafter, the sample with  $\sim 22$  nm Ag NPs is referred as Ag(h)/N-rGO and the results are mainly presented for this sample. For another case, the average size of the Ag NPs is  $\sim 70$  nm and is referred to Ag(l)/N-rGO.

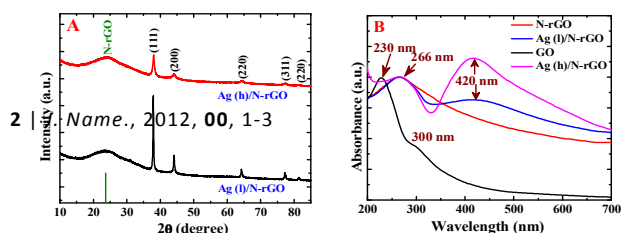


**Fig. 3** (A & B) XRD and UV-vis absorption spectra of hybrids.

The N-rGO sheets decorated with Ag NPs are characterized by XRD. XRD patterns shown in **Fig.3** A reveal five intense peaks at  $2\theta = 38^\circ, 44.25^\circ, 64.5^\circ, 77.26^\circ$  and  $81.54^\circ$ , which are assigned to (111), (200), (220), (311) and (222) planes of Ag (JCPDS No. 04-0783). Generally, GO shows a sharp peak at around  $2\theta = 11.5^\circ$ , which corresponds to d-spacing of 0.76 nm for (001) plane due to the presence of oxygen functionalities. The sharp peak corresponding to GO is absent and a broad peak appears at values  $2\theta = 24.5$  degree which is assigned to (002) plane of rGO (**ESI-2**). The d-spacing is estimated to be 0.36 nm which suggests the removal of large number of oxygen and functional group from GO (**ESI**). Overall, the results confirm the presence of Ag NPs in face-centered cubic (fcc) phase on N-rGO sheets. The reduction of GO and presence of Ag NPs is also confirmed by UV-visible spectroscopy as shown in **Fig. 3B**. In general, GO displays a strong peaks at 230 nm, corresponding to  $\pi$ - $\pi^*$  transitions of aromatic C-C bonds, and a weak peaks around 300 nm due to  $n$ - $\pi^*$  transitions of C=O bonds. The 230 nm peak is red shifted to 266 nm indicating the electronic conjugation within graphene sheet is recovered after reduction of GO.<sup>28-31</sup> A broad peak around 420 nm appeared for Ag(l)/N-rGO. This is the characteristic absorption peak of Ag NPs due to the surface plasmon resonance (SPR). When we increase the amount of Ag NPs on the graphene surface, the intensity of the SPR peak at  $\sim 420$  nm increased with a slight blue-shift of 4 nm which is in accordance with other reports.<sup>32, 33</sup>

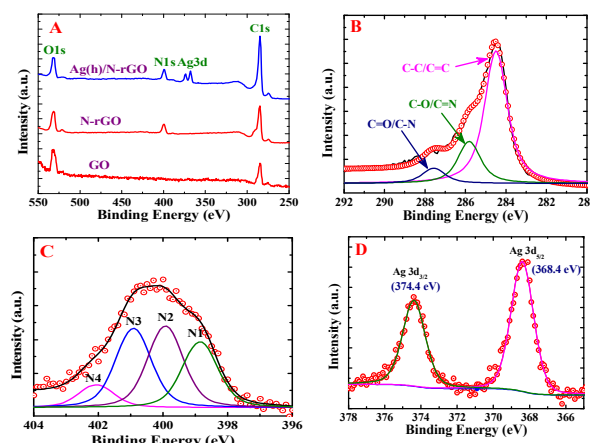


**Fig. 4** (A) XPS survey of GO, N-rGO and Ag(h)/N-rGO & spectra of (B) C 1s, (C) N 1s and (D) Ag 3d of Ag(h)/N-rGO sample.

XPS studies are carried out to determine the elemental composition along with their chemical state and also intuitively estimate the reduction level of GO and doping of N. **Fig. 4** (A) presents the survey XPS spectra of GO, N-rGO and Ag NPs/N-rGO hybrids. It can be noted for N-rGO that the peak corresponding to C1s increases confirming the reduction of GO. Furthermore, a peak



corresponding to N1s appears that confirm the doping of N. Similarly, reduction, doping and the formation of Ag NPs is realized from the XPS spectrum of Ag NPs/N-rGO. In order to estimate the reduction rate of GO, the C1s spectra (Fig. 4 B) were deconvoluted into three major peaks with the binding energy 284.5, 285.8 and 287.6 eV that corresponds to C-C/C=C ( $sp^2/sp^3$  bonding energy of carbon), C-O (epoxy, alcohol, ester and acid groups) and C=O (carbonyl groups), respectively. The most prominent peak corresponds to C-C (284.6 eV). The percentage of reduction were calculated by the area under the following three curves in C1s spectra and amount of the C-C bonds increases from 30 % to ~70 %, while the C-O and C=O bonds decreases from 50.6% to ~22 % and 19.4% to ~8 %, respectively. The doping of N was also confirmed by XPS. The binding energies of C-O and C-N bonds are very close and therefore, it is difficult to deconvolute the C1s spectra of N-rGO. However, the deconvolution of the high resolution XPS of N1s spectrum as shown in Fig. 4 C yields four major peaks that correspond to pyridinic N (N1= 398.7 eV), pyrrolic N (N2= 400 eV), quaternary N (N3= 401 eV) and N oxides of pyridinic N (N4=402.3 eV).<sup>7,23</sup> The area under the two peaks N1s and C1s is used to determine the percentage of N doping which also correlated with the energy dispersive X-ray spectra (ESI-3, Fig. 3 & 4). We can see that ~11% N was doped in rGO. Fig. 4 D represents the Ag 3d doublet of Ag NPs, where two bands at 368.4 eV and 374.4 eV are attributed to the binding energy of  $Ag3d_{5/2}$  and  $Ag3d_{3/2}$  electronic states, respectively. These two binding energy values are fairly higher than the of Ag metallic Ag (0), where this two energy states appear at 367.9 and 373.9 eV.<sup>34, 35</sup> These 0.5 eV higher binding energy shift can be described by the electron transfer from Ag NPs to rGO in the hybrids due to the lower work function of rGO (>4.8 eV) compared to Ag (4.2 eV). The purity of metallic Ag in the form of NPs was also confirmed by the 6 eV energy difference between the doublets of Ag 3d electronic states.<sup>36</sup>

The reduction of GO to N-rGO is also probed by micro Raman analysis (ESI-4). Both the GO and N-rGO are containing two major peak centred 1351 ( $A_{1g}$  vibrational mode, D band) and 1589  $cm^{-1}$  ( $E_{2g}$  vibrational mode, G band). The D band arises due to the defect and G peak corresponding to the graphitic peak. After the reduction of GO, the  $I_D/I_G$  intensity ratio slightly increases from 0.96 to 1.02 confirming the reduction of GO. The interaction of Ag NPs with N-rGO is further probed by SERS. The SERS can be achieved via two main reasons: (i) electromagnetic enhancement which is arise due to the SPR by physical interaction and (ii) chemical enhancement due to the formation of charge transfer complex via chemical bonding. It is interesting to note from Fig. 5A that the peak intensity of both the D and G band are enhanced by 180 % (1.8 fold) and 450 % (4.5 fold) when decorated with the Ag(l) and Ag(h) NPs. Overall, the enhancement factor is around 450 % for smaller NPs and 180% for bigger NPs. This low enhancement factor for Ag/N-rGO hybrids indicates the presence of a chemical interaction between the Ag NPs and N-rGO rather than electromagnetic enhancement.<sup>37, 38</sup> We also probe the Raman signal for Rhodamine 6G (Rh6G) and Rhodamine B (RhB). It can be noted from Fig. 5B that peaks around 612, 776, 934, 1135, 1192, 1314, 1367, 1425, 1510, 1579 and 1652  $cm^{-1}$  are in good agreement with earlier reports on Rh6G.<sup>39</sup>

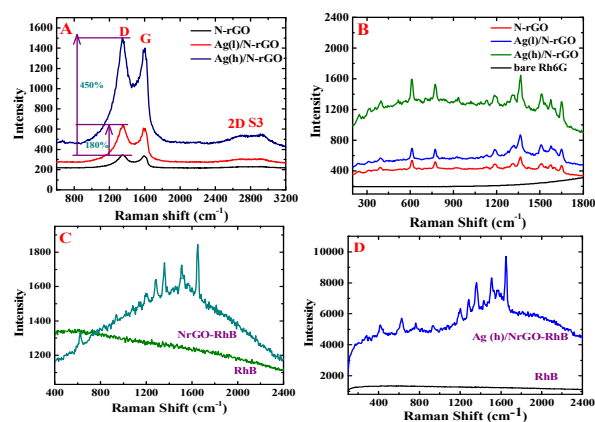


**Fig. 5** (A) The presence of Ag NPs enhances the native Raman spectra of N-rGO sheets by 180 and 450 %, characteristic for a chemical enhancement of N-rGO substrate. (B) Raman spectra of different hybrids nanostructures in presence of 100  $\mu M$  Rh6G probe molecule. (C & D) Raman spectra of RhB (100  $\mu M$ ) in presence of N-rGO and Ag(h)/N-rGO substrate. All samples are coated on soda lime glass.

Overall, though the enhancement is high for Ag(h)/N-rGO, N-rGO can also be used as metal-free SERS substrate. In the case of RhB,<sup>40</sup> the peaks at 624, 937, 1024, 1083, 1136, 1198, 1287, 1359, 1509, 1564 and 1650  $cm^{-1}$  are nicely seen through both N-rGO and Ag(h)/N-rGO as shown in Fig.5 (C & D), though the enhancement in the latter case is high. We have also investigated SERS of other probe molecules such as malachite green (MG) and congo red (CR) dye molecules (ESI-5).<sup>41</sup> It is believed that the Fermi energy level of N-rGO (4.8 eV) lies between the HOMO and LUMO energy levels of these dye molecules which facilitates  $\pi$ - $\pi$  bonding interaction via formation of charge transfer complex between the dyes and N-rGO. When for 4-mercapto benzoic acid (4-MBA) - a well-known SERS probe molecule on the metal substrate (Ag, Au etc.) is Raman inactive in presence of N-rGO as shown in ESI-. However, SERS is observed with Ag(h)/N-rGO as shown in ESI-. In this case, the energy difference between the HOMO (6.23 eV) - LUMO (1.29eV) are very high around 4.94 eV which doesn't favor the  $\pi$ - $\pi$  chemical interaction with the graphene. On the other hand, the bonding between thiol group (-SH) with the Ag is responsible for the SERS with Ag/N-rGO (ESI-5 Fig (E & F)).

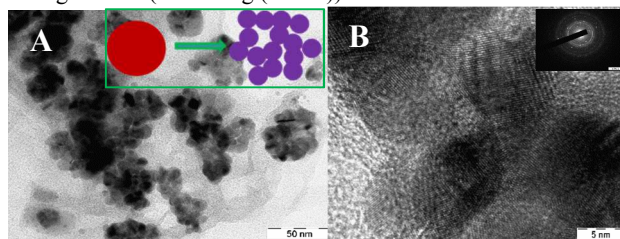


**Fig. 6** (A) shows the porous Pd nanostructures on N-rGO substrate by using Ag(h)/N-rGO as templates (inset shows the schematic of the Pd nanostructures) and Fig (B) shows the HRTEM images of ligand of the porous Pd (Inset images shows the SAED pattern).

We also synthesize Pd nanostructures by GRR using Ag(h)/N-rGO hybrids at room temperature. The standard reduction potential of  $E_{\text{Ag}^+/\text{Ag}}$  and  $E_{\text{Pd}^{2+}/\text{Pd}}$  is 0.80 and 0.90 V vs. standard electrode respectively. When  $\text{Pd}^{2+}$  ions are introduced into the hybrid solution, Pd nanostructures are obtained by sacrificing Ag NPs on N-rGO by following this chemical eqn.  $\text{Ag/N-rGO} + \text{Pd}^{2+} \rightarrow \text{Pd/N-rGO} + \text{Ag}^+$ . This is well supported by UV-vis and Raman spectroscopy (ESI-6). TEM and HRTEM images (Fig. 6 A & B) clearly confirm the porous structures of Pd which is larger than the size of the Ag NPs.

In conclusion, we report a one-step hydrothermal method for the synthesis of N-rGO and metal NPs decorated N-rGO hybrid nanostructures from GO, metal ions and HMT. The roles of HMT are to reduce the GO, the metal ions and the nitrogen source for doping rGO. We show that N-rGO as metal-free SERS substrate for the detection of various dyes molecules via chemical interaction. We also show that the hybrid nanostructures can be used as effective SERS substrate and template for decorating other various metallic nanostructures on N-rGO.

## Notes and references

<sup>a</sup> Materials Research Centre, Indian Institute of Science, Bangalore-560012, India. Fax: +91 80 2360 7316; Tel: +91 80 2293 2996; E-mail: [nanda@mrc.iisc.ernet.in](mailto:nanda@mrc.iisc.ernet.in)

† Electronic Supplementary Information (ESI) available: See DOI: 10.1039/b000000x/

1. Y. Zhu, S. Murali, W. Cai, X. Li, J.W. Suk, J. R. Potts, R.S. Ruoff, *Adv. Mater.* 2010, **22**, 3906-3924.
2. I.Y. Jeon, D. Yu, S. Y Bae, J. H. Choi, D. W. Chang, L. Dai, J. B. Baek, *Chem. Mater.* 2011, **23**, 3987-3992.
3. a) H. Sun, Y. Wang, S. Liu, L. Ge, L. Wang, Z. Zhu and S. Wang, *Chem. Commun.*, 2013, **49**, 9914-9916; b) D. Deng, X. Pan, L. Yu, Y. Cui, Y. Jiang, J. Qi, W. X. Li, Q. Fu, X. Ma, Q. Xue, G. Sun, X. Bao, *Chem. Mater.* 2011, **23**, 1188-1193.
4. X. K. Kong, C. L. Chen, Q. W. Chen, *Chem. Soc. Rev.* 2014, **43**, 2841.
5. L. Qu, Y. Liu, J. B. Baek, L. Dai, *ACS Nano*, 2010, **4**, 1321-1326.
6. Y. Liang, Y. Li, H. Wang, J. Zhou, J. Wang, T. Regier, H. Dai, *Nat. Mater.*, 2011, **10**, 780-786.
7. Y. Shao, S. Zhang, M. H. Engelhard, G. Li, G. Shao, Y. Wang, J. Liu, I. A. Aksay, Y. Lin, *J. Mater. Chem.* 2010, **20**, 7491-7496.
8. X. Ling, L. Xie, Y. Fang, H. Xu, H. Zhang, J. Kong, M.S. Dresselhaus, J. Zhang, Z. Liu, *Nano Lett.* 2009, **10**, 553-561.
9. W. Xu, N. Mao, J. Zhang, *Small*. 2013, **9**, 1206-1224.
10. W. Xu, X. Ling, J. Xiao, M.S. Dresselhaus, J. Kong, H. Xu, Z. Liu, J. Zhang, *Proceedings of the National Academy of Sciences*. 2012, **109**, 9281-9286.
11. W. Xu, J. Xiao, Y. Chen, Y. Chen, X. Ling, J. Zhang, *Adv. Mater.* 2013, **25**, 928-933.
12. X. K. Kong, Z. Y. Sun, M. Chen, C.L. Chen, Q.W. Chen, *Energy & Environmental Science*, 2013, **6**, 3260-3266.
13. H. K. Sadhanala, J. Khatei, K. K. Nanda, *RSC Adv.*, 2014, **4**, 11481-11485.
14. Novoselov, K. S.; Geim, A. K.; Morozov, S. V.; Jiang, D.; Zhang, Y.; Dubonos, S. V.; Grigorieva, I. V.; Firsov, A. A., *Science* 2004, **306**, 666-669.
15. K. S. Kim, Y. Zhao, H. Jang, S. Y. Lee, J. M. Kim, K. S. Kim, J. H. Ahn, P. Kim, J. Y. Choi, B. H. Hong, *Nature* 2009, **457**, 706-710.
16. P. W. Sutter, J. I. Flege, E. A. Sutter, *Nat. Mater.* 2008, **7**, 406-411.
17. S. Stankovich, D. A. Dikin, R. D. Piner, K. A. Kohlhaas, A. Kleinhammes, Y. Jia, Y. Wu, S. T. Nguyen, R. S. Ruoff, R. S., *Carbon* 2007, **45**, 1558-1565.
18. S. Park, R. S. Ruoff, *Nat Nano.* 2009, **4**, 217-224.
19. V. C. Tung, M. J. Allen, Y. Yang, R. B. Kaner, *Nat Nano.*, 2009, **4**, 25-29.
20. X. Li, H. Wang, J. T. Robinson, H. Sanchez, G. Diankov, H. Dai, *J. Am. Chem. Soc.* 2009, **131**, 15939-15944.
21. Z. Jin, J. Yao, C. Kittrell, J. M. Tour, *ACS Nano*, 2011, **5**, 4112-4117.
22. (a) J.W. Lee, J. M. Ko, J. D. Kim, *Electrochimica Acta*, 2012, **85**, 459-466; (b) X. Shen, L. Jiang, Z. Ji, J. Wu, H. Zhou, G. Zhu, *Journal of Colloid and Interface Science*, 2011, **354**, 493-497.
23. a) S. Maldonado, S. Morin, K. J. Stevenson; *Carbon*, 2006, **44**, 1429-1437; b) H. Wang, T. Maiyalagan, X. Wang, *ACS Catalysis* 2012, **2**, 781-794; (c) Z. H. Sheng, L. Shao, J. J. Chen, W. J. Bao, F. B. Wang and X. H. Xia, *ACS Nano*, 2011, **5**, 4350-4358.
24. a) L. Sun, L. Wang, C. Tian, T. Tan, Y. Xie, K. Shi, M. Li and H. Fu, *RSC Adv.*, 2012, **2**, 4498-4506; b) D. Yu, J. Yao, L. Qiu, Y. Wu, L. Li, Y. Feng, Q. Liu, D. Lic and H. Wang, *RSC Adv.*, 2013, **3**, 11552-11555; c) Z. Lin, M. K. Song, Y. Ding, Y. Liu, M. Liu, C. P. Wong, *Phy. Chem. Chem. Phy.* 2012, **14**, 3381-3387.
25. E. Yoo, J. Kim, E. Hosono, H. Zhou, T. Kudo, I. Honma, *Nano Letters* 2008, **8**, 2277-2282.
26. j. Tian, S. Liu, Y. Zhang, H. Li, L. Wang, Y. Luo, A. M. Asiri, A. O. Al-Youbi, X. Sun, *Inorganic Chemistry* 2012, **51**, 4742-4746.
27. Z. Zhang, F. Xu, W. Yang, M. Guo, X. Wang, B. Zhang, J. Tang, *Chem. Commun.* 2011, **47**, 6440-6442.
28. Z. Fan, K. Wang, T. Wei, J. Yan, L. Song, B. Shao, *Carbon* 2010, **48**, 1686-1689.
29. Z. J. Fan, W. Kai, J. Yan, T. Wei, L.J. Zhi, J. Feng, Y. M. Ren, L. P. Song, F. Wei, *ACS Nano* 2010, **5**, 191-198.
30. B. K. Barman, P. Mahanandia, K. K. Nanda, K. K., *RSC Adv.*, 2013, **3**, 12621-12624.
31. Y. Zhu, W. Cai, R. D. Piner, A. Velamakanni, R. S. Ruoff, *App. Phys. Lett.* 2009, **95**, 123115.
32. X. Z. Tang, Z. Cao, H. B. Zhang, J. Liu, Z. Z. Yu, *Chem. Commun.* 2011, **47**, 3084-3086.
33. J. Li, C. Y. Liu, *European Journal of Inorganic Chemistry*, 2010, **8**, 1244-1248.
34. V. G. Pol, D. N. Srivastava, O. Palchik, V. Palchik, M. A. Slifkin, A. M. Weiss, A. Gedanken, *Langmuir*. 2002, **18**, 3352-3357.
35. T. Wu, H. Shen, L. Sun, B. Cheng, B. Liu, J. Shen, *ACS Applied Materials & Interfaces* 2012, **4**, 2041-2047.
36. S. Dutta, C. Ray, S. Sarkar, M. Pradhan, Y. Negishi, T. Pal, *ACS Applied Materials & Interfaces* 2013, **5**, 8724-8732.
37. K. Jasuja, V. Berry, *ACS Nano.*, 2009, **3**, 2358-2366.
38. K. Jasuja, J. Linn, S. Melton, V. Berry, *J. Phys. Chem. Lett.* 2010, **1**, 1853-1860.
39. a) Z. Yuda, X. Yizh, B. Zhiyong, H. Yuen, T. Hong Tsang, X. Liming, C. Yang Chai, *J. Phys. Chem. C*, 2014, **118**, 11827-11832; b) R. Lv, Q. Li, A. R. Botello-Méndez, T. Hayashi, B. Wang, A. Berkdemir, Q. Hao, A. L. Elías, R. Cruz-Silva, H. R. Gutiérrez, *Sci. Rep.* 2012, **2**, 586.

## Journal Name

40. X. Yu, H. Cai, W. Zhang, X. Li, N. Pan, Y. Luo, X. Wang, J. G. Hou, *ACS Nano*, 2011, **5**, 952–958.
41. J. Yue, M. Pinyi, L. Fanghui, G. Dejiang, W. Xinghua, *Anal. Methods*, 2013, **5**, 5609-5014.

# Hexamethylenetetramine mediated simultaneous nitrogen doping and reduction of graphene oxide for a metal-free SERS substrate

By Barun Kumar Barman and Karuna Kar Nanda\*

We report a one-pot hydrothermal synthesis of nitrogen doped reduced graphene oxide (N-rGO) and Ag nanoparticles decorated N-rGO hybrid nanostructures from graphene oxide (GO), metal ions and hexamethylenetetramine (HMT). HMT not only reduces GO and metal ions simultaneously but also acts as the source for the nitrogen (N) dopant. We show that the N-rGO can be used as metal-free surface enhanced Raman spectroscopy (SERS) substrate, while the presence of Ag nanoparticles (NPs) decorated N-rGO can be used for further enhancement of SERS. We also show that Ag NPs/N-rGO is used for template for decorating various other noble metals on N-rGO.

